Full orbit simulations of ion collisional and turbulent transport in the MAST spherical tokamak

M Romanelli[1], K G McClements[1], J Cross[2], P J Knight[1], A Thyagaraja[1], J Callaghan[3]

[1]EURATOM/CCFE Fusion Association, Culham Science Centre, Abingdon, Oxon, OX14 3DB, UK
[2]University of Bath, Bath BA2 7AY, UK
[3]University of Oxford, New College, Oxford, UK

E-mail: michele.romanelli@ccfe.ac.uk

Abstract

Transport analysis of MAST discharges indicates that ion collisional transport is an important loss mechanism in the core of a spherical tokamak. In the strongly-varying equilibrium fields of spherical tokamaks many of the assumptions of drift kinetic and neoclassical theory (e.g. small plasma inverse aspect ratio and low ratio of toroidal Larmor radius to poloidal Larmor radius) are often not valid. In these circumstances it is appropriate to use a full ion-orbit analysis to evaluate heat and particle fluxes. Both collisional and turbulent transport have been investigated in MAST conditions using a full ion-orbit solver, CUEBIT, to track test-particles in steady-state and fluctuating fields computed using cylindrical and toroidal two-fluid electromagnetic turbulence codes, CUTIE and CENTORI. A study of the scaling of ion diffusivity with collisionality reveals deviations from the standard neoclassical theory, in both the Pfirsch-Schlüter and banana regimes, and difficulties in defining a local diffusivity at low collisionalities. The inclusion of field fluctuations along with collisions is found to enhance the non-diffusive nature of particle transport. The full orbit analysis predicts levels of transport and confinement times broadly consistent with experimental observations.

1. Introduction

Transport analysis of plasmas in the MAST spherical tokamak [1] show that, while electron conductivities are largely "anomalous" all over the discharge, ion conductivities in the plasma core (over up to 60% of the minor radius) have values not far from those predicted by the standard neoclassical theory [2-4]. This experimental evidence suggests that collisional transport can be an important loss mechanism in spherical tokamaks and that it is necessary to re-examine the fundamental assumptions of the neoclassical theory, in light of the parameters pertaining to this configuration. Indeed collisional transport in spherical tokamaks, where the toroidal component of the confining magnetic field is of the same order of the poloidal component at the low field side, is not expected to be correctly described by the standard neoclassical ordering [5] based on an expansion in the drift parameters ($\varepsilon = a/R << 1;\ B_\theta / B_\phi << 1$ where a and R are the plasma minor and major radii, and B_θ and B_ϕ the poloidal and toroidal components of the confining magnetic field respectively). Previous analytical and numerical results have highlighted the fact that tight aspect ratio tokamaks can exhibit non-local collisional transport [6] along with deviations from the neoclassical ordering that can only be captured by a full orbit particle analysis [7]. Moreover in the presence of toroidally-

asymmetric time-dependent field fluctuations (turbulence) neither toroidal angular momentum nor particle energy is conserved, and for fluctuations with sufficiently short wavelength the magnetic moment may cease to be an adiabatic invariant. In view of the considerations above, in order to compute accurately collisional and turbulent transport of heat and particles in the fluctuating fields of a spherical tokamak it is appropriate to go beyond drift kinetic theory and integrate the full particle orbits. In this framework transport and confinement of ions in the MAST spherical tokamak has been studied with a full orbit particle code CUEBIT [8] coupled to two global electromagnetic turbulence and transport codes CUTIE [9] and CENTORI [10].

The CCFE spherical tokamak MAST has major radius R = 0.85 m and minor radius a = 0.65 m, hence inverse aspect ratio $a/R \approx 0.8$. The typical toroidal magnetic field at the magnetic axis is 0.6 T and the typical plasma current is 1 MA. The main heating system is neutral beam injection, with presently powers up to about 3.5 MW achieved. The beam introduces a large population of fast deuterons into the plasma (with concentration n_{fD}/n_e ~10% where n_{fD} indicates the density of the energetic deuterium and n_e the electron density) with nominal energy peak at 70 keV. Carbon and oxygen are the most abundant impurities with concentrations around n_C/n_e ~ 5% and n_O/n_e ~ 1% respectively. The ion temperatures achieved routinely in the plasma core are of the order of 1 keV. With the above plasma parameters typical values of the Larmor radii of deuterons (thermal, energetic), carbon ions and oxygen ions are respectively. ρ_D ~ 1.0 cm, ρ_{fD} ~ 8 cm (where 40 keV deuterium ions have been assumed), $\rho_{C,O}$ ~ 2.5-3.0 cm. At mid-radius (r/a=0.5 where r is a radial position ranging between 0 and a) in a typical MAST discharge, the ion orbit widths for these species are of the same order as the Larmor radius. The typical gradient scale-lengths of temperature, density and safety factor are $L_{T,n,q}$ = 0.3 m at mid radius, dropping to around 0.2 m at r/a=0.8 [11].

The paper is organized as follows. In the next section the particle following code CUEBIT is briefly described, along with the scheme used to couple the code with those providing the equilibrium and fluctuating electromagnetic fields. In section 3 results on collisional transport in MAST equilibrium magnetic field are presented, and in section 4 the effects of the equilibrium radial electric field and electromagnetic field fluctuations on particle transport are discussed. Our conclusions are presented in section 5.

2. Particle orbit integration scheme

In this paper ion transport is investigated numerically by initialising a population of test particles on a given magnetic surface and following their full orbits in the prescribed equilibrium and fluctuating electromagnetic fields, taking into account collisional interactions with a flowing ion species. We assume that the measured transport of the test particles belonging to a particular species is representative of the bulk transport of that species within the background plasma. This method can be regarded as a numerical simulation of a beam injection or laser blow off experiment, which can be used to obtain direct information on particle transport [12]. The CUEBIT code is used to solve the Lorentz force equation for charged particles in arbitrary time-varying electric and magnetic fields using an algorithm that ensures conservation of total energy to machine accuracy when $\boldsymbol{E} = \mathbf{0}$ [13]. The equilibrium magnetic field expressed in terms of a poloidal-flux function $\psi(R,Z)$ and a toroidal magnetic field along with the equilibrium electric field, plasma velocity and fields fluctuations are calculated using the two-fluid transport and turbulence codes CUTIE (cylindrical, circular equilibrium) and CENTORI (fully toroidal, shaped magnetic surfaces). For the case in which $\boldsymbol{E}$ is a potential field, the total energy of collisionless particles is generally conserved to a satisfactory level of accuracy by taking the time step to be around a tenth of a Larmor period. In the laboratory frame the Lorentz force equation then takes the form

$$m\frac{d\mathrm{v}}{dt} = Ze\left(\mathrm{E} + \mathrm{v}\times\mathrm{B}\right) - \frac{m}{\tau}\left(\mathrm{v} - \mathrm{V}\right) + m\mathrm{a}_{\mathrm{r}} \qquad (1)$$

The electric and magnetic fields as well as the plasma velocity **V** include both the equilibrium (slowly varying) and the fluctuating (rapidly varying in time and space) components:

$$\mathrm{E} = \mathrm{E}_0(\psi,t_0) + \delta\mathrm{E}_1(\psi,\theta,\varphi,t_1);\ \ \mathrm{B} = \mathrm{B}_0(\psi,t_0) + \delta\mathrm{B}_1(\psi,\theta,\varphi,t_1);\ \ \mathrm{V} = \mathrm{V}_0(\psi,t_0) + \delta\mathrm{V}_1(\psi,\theta,\varphi,t_1)$$

In the above expressions we have adopted toroidal coordinates with toroidal angle φ and poloidal angle θ. The equilibrium fields are taken to vary on the energy confinement time scale while the rate of variation of the fluctuating components is assumed to be of the order of the ion diamagnetic frequency (10-500 kHz). The use of different time variables t_0 and t_1 in the above expression reflects these different timescales. The flux surface averages of the rapidly varying components of the fields are generally small compared to the equilibrium fields; when this condition is broken, a transition to a new equilibrium may occur and the large fluctuation becomes part of the new equilibrium (examples include L-H transitions, ITB formation, sawtooth crashes). The parameter $\tau = \tau(\psi, t_1)$ is a collision time (in the case of trace impurities it is assumed to be velocity independent while depending on the equilibrium plasma parameters) and $\mathrm{a}_r(\psi, t_1) = (\mathrm{a}_{r\,x}, \mathrm{a}_{r\,y}, \mathrm{a}_{r\,z})$ is a set of random numbers, chosen independently for each particle and at each time step, with zero mean and standard deviation equal to the thermal velocity of the background plasma ions divided by the geometric mean of the collision time and the time step δt used to follow the particle $\sigma = (2T_i(\psi, t_1)/m)^{1/2}/\sqrt{\tau \delta t}$ [8]. The presence of noise terms in the three components of equation (1) ensures that collisional pitch angle scattering is taken into account. For the case of a Maxwellian distribution of field particles the collision time τ is given by the expression

$$\frac{1}{\tau} = \frac{m_i^{1/2}}{m} \frac{Z^2 Z_i^2 e^4 n_i(\psi, t_1) \ln \Lambda}{6\sqrt{2}\pi^{3/2} \varepsilon_0^2 T_i^{3/2}(\psi, t_1)} \tag{2}$$

where the index i denotes the scattering ions of the background plasma, e is the proton charge, $\ln\Lambda$ is the Coulomb logarithm, T denotes temperature and ε_0 is the permittivity of free space. Note that in the absence of fluctuating fields the test particles are influenced by the background plasma both through the collision frequency (which depends on the position of the test particle) and through the plasma velocity and equilibrium electric field. The latter is taken to be the electric field which confines the background ions, as calculated from the ion momentum-balance equation

$$\mathrm{E}_0(\psi, t_0) = \frac{m_i}{e} \mathrm{V}_0 \cdot \nabla \mathrm{V}_0 + \frac{1}{n_i e} \nabla p_{i0} - (\mathrm{V}_0 \times \mathrm{B}_0) + \eta \mathrm{j}_0 \tag{3}$$

Where j_0 is the equilibrium current density. The last term on the right hand side of equation (3) is associated with the toroidal component of the equilibrium electric field $E_\varphi = \eta j_\varphi$, and is responsible for the Ware pinch.

The two-fluid global electromagnetic turbulence codes CUTIE and CENTORI resolve the spectrum of fluctuations with poloidal and toroidal mode numbers m = 0-64, n = 0-32 (with typically 100 radial grid points) on a time scale of the order of the Alfvén time. They differ in the geometry, being CUTIE circular cylindrical and CENTORI fully toroidal. The coupling of CUEBIT with CUTIE/CENTORI has been achieved both dynamically (i.e. with test-particle orbits being computed simultaneously with fluctuating fields) and in post-processing mode. Since the test-particles do not affect the dynamics of the background plasma, the post-processing mode is the most effective in terms of time required for running the simulations and it allows the possibility of repeating the simulations to probe transport in different regions of the plasma and with different particle species. In the post-processing mode CUTIE and CENTORI are run separately, and the full 3D magnetic field, electric field and velocity field are stored in an intermediate file at simulated time intervals $\Delta t_C = 10/\omega_{ci}$ (where ω_{ci} is the plasma ion cyclotron frequency). The file is then reduced by a postprocessor calculating at each time step and toroidal position an expansion in terms of Chebyshev polynomials, which ensures the best approximation of the function for a chosen polynomial degree. A general field-component a is then expanded as

$$a[\psi(R,Z), \theta(R,Z), \varphi, t_1] = \sum_{s,l=0}^{n}{}'' a_{sl}(\varphi, t_1) T_s(R) T_l(Z) \tag{4}$$

where the Chebyshev polynomials of the first kind are defined by the recurrence relation

$$T_0(x) = 1; \quad T_1(x) = x; \quad T_{n+1}(x) = 2xT_n(x) - T_{n-1}(x) \tag{5}$$

The coefficients $a_{sl}(\varphi, t_1)$ are stored in a data file. The maximum degree of the fitting polynomial, *n*, is chosen accordingly with the number of grid points at which the field is given (depending on the numerical grid). Once the data file is ready, particle trajectories can be computed with CUEBIT. At the beginning of the particle loop cycle, after initializing the particle position and velocities, CUEBIT imports from the data file the coefficients $a_{sl}(\varphi, t_1)$ for each field component at two successive times ($t=0$ and $t=\Delta t_C$). The trajectories of the particles are then calculated in the time interval Δt_C with time step δt typically one tenth of the particle Larmor time (this might differ for each particle), where $\delta t << \Delta t_C$. The fields at each particle position and time step are computed by linearly interpolating in time and toroidal angle the coefficients $a_{sl}(\varphi, t_1)$ in the polynomial expansion. Once the particles have been advanced for a time Δt_C the coefficients for the next time interval are loaded and the procedure is carried on till the end of the simulation. As discussed in the next section, the number of iterations necessary for calculating the local diffusion coefficients varies with collisionality. Particles reaching 95% of the plasma minor radius are counted as lost and removed from the simulation. The particle confinement time is calculated by following the test particles until their total number has dropped by a factor of *e*. Confinement times in MAST conditions are typically a few tens of milliseconds. The most demanding CUEBIT runs discussed in this paper have been performed with a parallel version of the code, following the orbits of 10^4 particles on 10^3 processors (10 particles per processor) for 50 ms and time step 10^{-8} s. The positions and velocities of the particles are periodically stored in an output file, together with statistical information such as the average displacement of the ensemble of particles from the initial magnetic surface and the mean square displacement. Diffusion coefficients, advection velocities and confinement times are then obtained by analysing the output, as explained in the next section.

3. Collisional transport in the MAST tokamak

In this paper we will make use of two orthogonal coordinate systems: Cartesian coordinates (*x,y,z*); cylindrical coordinates ($R = \sqrt{x^2 + y^2}$, $\varphi = \arctan y/x, Z = z$ where the axis of the cylinder coincides with the torus symmetry axis); and the non-orthogonal toroidal coordinates $\psi = \psi(R,Z); \theta = \theta(R,Z), \varphi = \varphi$. The functions ψ, θ, φ will be referred to as flux function, poloidal angle and toroidal angle respectively. In general the flux function ψ is chosen to be negative at the magnetic axis and equal to zero at the plasma boundary. In the case of a circular cross section plasma a good choice of toroidal coordinates is $\psi = \psi\left((R^2 - R_0)^2 + Z^2\right), \theta = \arctan Z/(R - R_0), \varphi = \varphi$ where the flux coordinate is a function of the minor radius of the circular magnetic surface. Local transport analysis is carried out by positioning the test particles on a chosen magnetic surface, denoted with $\psi(R,Z) = \psi_0$, and at the same poloidal and toroidal angles θ_0, φ_0 . Thus the initial spatial distribution of test particles is given by

$$n(\psi, \theta, \varphi, t_0) = J_0 N_0 \delta(\psi - \psi_0) \delta(\theta - \theta_0) \delta(\varphi - \varphi_0) \tag{6}$$

where $J_0 = \left|\nabla\theta \times \nabla\psi . \nabla\varphi\right|_0$ is the inverse of the element of volume in the chosen toroidal coordinates calculated at $\psi_0, \theta_0, \varphi_0$. The three components of the initial velocities are chosen by sampling randomly a Gaussian distribution with zero mean and standard deviation equal to the thermal velocity of the represented species (e.g. fuel ions, fast ions, impurities). Alternatively, the particles can be initialised with the same initial energy and a uniform distribution of randomly chosen pitch angles; after few collision times the particles are fully thermalised and have a Maxwellian distribution with a temperature equal to that of the background ions. The particle trajectories are then calculated without

collisions [i.e. with the two inertial terms on the right hand side of equation (1) switched off] for a few passing particle toroidal transit times or trapped particle bounce times, to allow the particles to become distributed all over their drift surfaces around the initial magnetic surface (this process is better optimized when the particles are chosen initially to have the same energy). During this short initial time the particles drift from the initial magnetic surface and position themselves on a range of drift orbits. This initial radial expansion (here "radial" refers to the direction locally perpendicular to the magnetic surface) is a ballistic process that must be filtered out from the diffusive and convective transport processes that we aim to study. In the absence of collisions and fluctuations the particles would remain on their drift surfaces and their average radial position would be constant in time. We define the particle's average position and mean displacement as follows:

$$\bar{r}(t) = \frac{1}{N_0}\sum_i r_i(t)\ ,\ \ \Delta r(t) = \frac{1}{N_0}\sqrt{\sum_{i=1,N_0}\left(r_i(t) - \bar{r}(t)\right)^2} \tag{7}$$

where $r_i = r_i\left(\psi_i(t)\right) = a\sqrt{1 - \psi_i(t)/\psi_{axis}}$, is the radial position (in length units) of the i-th particle and ψ_{axis} is the value of the flux function at the position (R,Z) of the magnetic axis. Figure 1 shows the drift orbit of three particles in the initial distribution, computed without collisions or electric fields, and figure 2 shows the distribution of particles around the starting magnetic surface. Figure 1 illustrates the fact that, due to finite Larmor radius effects, the total orbital excursions of trapped ions in spherical tokamaks can be significantly greater than their guiding centre orbit widths; as noted by Gates and co-workers [7], this leads to an enhanced diffusivity for example in the banana regime of neoclassical transport.

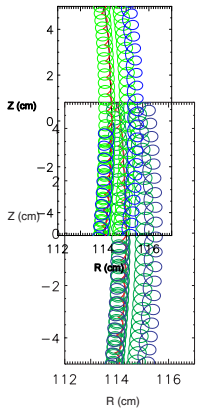

Figure 1. Close-up of the drift orbits of three particles on the low field side of a MAST-like plasma. Two of the particles (green and blue trajectories) are trapped and one (red trajectory) is passing. The black line shows the position of the starting magnetic surface.

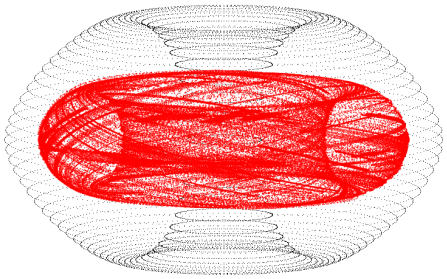

Figure 2. Collisionless trajectories of 10^2 particles around the starting magnetic surface in a MAST-like equilibrium. The light (grey) curves indicate the plasma boundary.

Successively the collision terms in equation (1) are turned on and the scattered trajectories calculated. In order to determine the scaling with collisionality of the local ion diffusivity and convective velocity, the evolution of the test-particle distribution must be followed for a time Δt_{local} that is short enough to ensure that the particles have not been transported too far from the initial radial position, since the transport coefficient varies in space. On the other hand it is necessary to follow the trajectories for a time Δt_v that is long enough that well-defined transport coefficients can be inferred from spatial moments of the test-particle distribution; typically Δt_v must be at least several collision times [14]. The condition for transport to be local (e.g. entirely ascribable to local parameters and field gradients) is therefore $\Delta t_v << \Delta t_{local}$. When the collision time is chosen to be much shorter than the passing particle circulation time or the trapped particle bounce time then the particles do not travel far from their initial position on the magnetic surface and they are not subject to significant grad-**B** or curvature drifts (responsible for the effects of toroidal geometry on collisional transport). In this case we recover classical transport. By increasing the collision time to a value longer than the average circulation time of passing particles but shorter than the average trapped particle bounce time, the test particles on average sample a significant fraction of the magnetic surface before undergoing a collision, and the geometry (through the grad-**B** and curvature drifts) starts to influence the diffusivity. By increasing further the collision time to few bouncing times, a fraction of the test particles have closed banana orbits and the diffusion process is affected by the appearance of radially-extended orbits and collisional pitch-angle scattering of particles close to the bounce points of trapped orbits (when the parallel particle velocities approach zero). The scan in collisionality described above has been performed by eliminating field fluctuations and the electric field and positioning 10^4 ions at r/a=0.5 in both a CUTIE circular equilibrium and in CENTORI elongated equilibrium. The use of a reduced number of particles is allowed by the fact that the analysis is local in both radial position and time. A convergence study has been carried out by varying the number of particles between 10^3 and 10^6. As expected the noise on the time dependence of the mean square displacement scales inversely with the square root of the number of particles. The use of 10^4 particles is found to provide a good estimate of the local transport coefficients. We will discuss now four study cases.

As a first step we have benchmarked CUEBIT against the neoclassical analytical results in the large aspect ratio limit. We have considered a low beta, circular cross section plasma with inverse aspect ratio a/R_0 = 0.1 (R_0=10 m, a =1 m). The toroidal component of the magnetic field is taken as $B_\varphi=B_0R_0/R$, (B_0=1.0 T) and the poloidal component of the equilibrium field is calculated for a plasma with $q(a)$ = 4.0 (I_p = 121 kA, B_φ(0.5a) = 0.035T , $q(0.5a)$=1.4). The test particles (N_0=10^4, A = 12, Z = 6, i.e. fully ionized carbon) are placed initially at $r_i/a = r_0/a$ = 0.5. Random toroidal angles (uniformly distributed) and constant poloidal angle (equal to zero) are chosen as initial conditions; the initial particle distribution is thus $n(r,t_0)=(1/2\pi r_0(R_0+r_0))N_0\delta(r-r_0)\delta(\theta)$. This choice of the initial positions and velocity distribution ensures that the fraction of trapped particles in the simulation is correctly represented (the fraction of trapped particles in the large aspect ratio limit is proportional to the square root of the inverse aspect ratio). The gyrofrequency and Larmor radius of each individual particle depends on its initial position and perpendicular velocity. For the chosen magnetic field the gyrofrequency ranges from ω_{ci} = 4.5×10^7 s^{-1} on the low field side to ω_{ci} = 4.9×10^7 s^{-1} on the high field side (this variation can be neglected in the large aspect ratio limit). Particle trajectories, $r_i(t),\theta_i(t),\varphi_i(t)$, are calculated solving the stochastic equations (1) described in the previous section for a time exceeding several collision times τ (typically 50τ).

Particles are transported radially by collisions. For short times such that $\Delta r(t)/r << 1$ and $(\bar{r}-r_0)/r_0 << 1$ the evolution of the radial distribution is described by

$$n(t,r)=\frac{N_0}{\sigma(t)\sqrt{2\pi}}e^{\frac{[r-\bar{r}(t)]^2}{2\sigma^2}}, \tag{8}$$

where $\sigma=\sqrt{2D(t-t_0)}$, D being the diffusion coefficient appearing in the transport equation

$$\frac{\partial n}{\partial t}=D\frac{\partial^2 n}{\partial r^2}+V\frac{\partial n}{\partial r}, \tag{9}$$

where V is a convective velocity. We can determine the diffusion coefficient from the particle distribution by computing $\Delta r^2 \approx \sigma^2 = 2D(t-t_0)$, with Δr defined in equation (7), while any time variation in $\bar{r}$ indicates convection. Our first objective is to determine how D scales with the collision time τ in the given equilibrium magnetic field. As mentioned above, in order to resolve the Larmor orbit we use a time step ten times smaller than the shortest cyclotron period. Different values of collisionality $\nu^* = Rq\nu / V_{th}$ are accessed by varying the collision time at constant thermal velocities V_{th} (and Larmor radii). In order to access the banana regime with a thermal velocity of the order of 10^4 ms^{-1} the collision time has to exceed 10^{-2} s. Having to compute more than 10 collision times requires the calculation to be carried out for a time between 0.1 s and 1 s while the Pfirsch-Schlüter (P-S) regime requires short simulations of less than 0.1 ms.

For the first case study (small Larmor radius, large aspect ratio $R=10$ m, $a=1$ m, $A/Z = 2$) we have chosen a thermal velocity of 3.4×10^4 ms^{-1} (corresponding to a Larmor radius $\rho = 0.7\times10^{-3}$ m) and varied the collision time by 7 orders of magnitude, with the smallest value equal to the cyclotron period. In figure 3 the diffusion coefficients calculated with CUEBIT are compared at highly collisionality with the expected classical values $D_{cl} = \left\langle \left\langle \rho^2 \right\rangle_v \right\rangle_{\theta\varphi} / 2\tau$, (where the two brackets indicate velocity space average and magnetic surface average $\left\langle \left\langle \rho^2 \right\rangle_v \right\rangle_{\theta\varphi} = \bar{\rho}^2 = 2(mV_{th}/ZeB_\theta)^2$ and $V_{th} = (T_i/m)^{1/2}$) and at lower collisionalities ($\nu^* < 5$) with the P-S diffusion coefficient $D_{ps} \approx (1+2q^2)\bar{\rho}^2/2\tau$, where q=1.4.

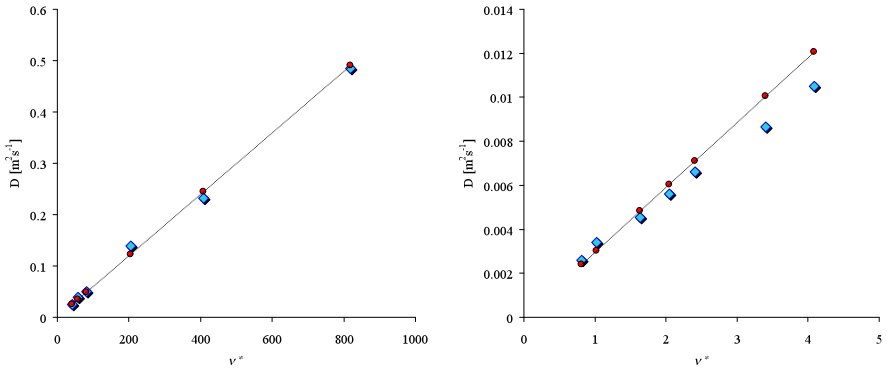

Figure 3. Computed diffusivity (diamonds) versus collisionality in the classical (left plot) and P-S regimes (right plot) for small Larmor radius particles ($\rho = 0.7\times10^{-3}$ m and thermal velocity of 3.4×10^4 ms^{-1}, in a conventional aspect ratio tokamak ($R_0/a=10$). The red circles indicate the expected value of the diffusivity, D_{cl} and D_{PS} respectively. The divergence of the simulated and predicted diffusivities around ν*=5 indicates a transition from P-S to classical scaling.

Banana regime scaling is expected for $\nu^* < \varepsilon^{3/2} = 0.01$. However, for the chosen value of the Larmor radius the expected diffusion coefficient in the banana regime ($D_B \approx \varepsilon^{-3/2} q^2 \bar{\rho}^2 / 2\tau$) is of the order of 10^{-4} m^{2}s^{-1} or smaller and would require long simulation with a larger number of particles (lower noise) to resolve it properly. We will therefore discuss the banana regime in the next case study where a Larmor radius ten times larger has been chosen. For all values of collisionality used in the first case study the relative displacement of the average of the particle distribution was negligible, between 10^{-3} and 10^{-2}.

For the second case study (larger Larmor radius, large aspect ratio, A/Z=2) we have repeated the scan above for ions having a thermal velocity of 4.8×10^5 ms^{-1}, corresponding to an average Larmor radius of 1 cm (1.06 cm on the low field side, 0.97 cm on the high field side). The collision time required to access the banana regime for this choice of parameters is one order of magnitude smaller (4×10^{-3} s) and the collisionality regime can be accessed promptly with a smaller number of iterations. The scaling of the calculated diffusion coefficient with collisionality in the P-S and banana regime is reported in figure 4.

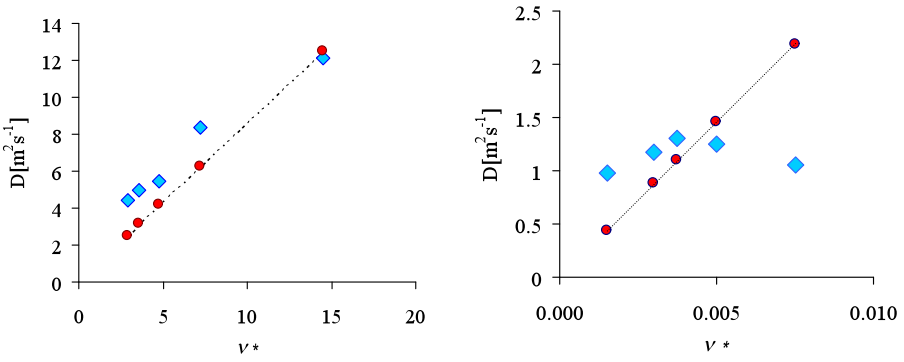

Figure 4. Computed diffusivity (diamonds) versus collisionality in the P-S (left plot) and banana (right plot) regimes for larger Larmor radius ions (ρ=1 cm, V_{th} =4.8×10^5 ms^{-1}) in a conventional aspect ratio tokamak ($R_0/a=0.1$). The red circles indicate the value of the corresponding expected neoclassical diffusion coefficient, respectively D_{PS} and D_B.

kmcc 13/8/10 12:06
Comment: The neoclassical diffusion coefficients in the right hand plot are way too low!

In the low collisionality regime we observe a collisional radial-drift (pinch velocity) $\mathbf{V}_{cD}$ of the peak of the particle distribution which scales with the square of the Larmor radius. The component parallel to the magnetic surface of the curvature and centrifugal drifts produce a radial drift through the drag term of equation (1) ($V_{cD} = -m(v_{\nabla B}\times B/ZeB^2)/\tau$ where $v_{\nabla B} = \rho V_{th}\nabla B\times B/B^2$; defining $1/L_B = \left|\nabla B\times B/B^2\right|$ we thus have $\left|V_{cD}\right| = \rho^2/L_B\tau$) that quickly takes the particles away from the initial surface, well before diffusion begins to modify the particle distribution. Therefore the transport at this level of collisionality is non diffusive and non local. By linearly interpolating $\Delta r^2(t)$ between 30 and 50 collision times we obtain an effective diffusion coefficient that can be compared with the neoclassical $D_B \approx \varepsilon^{-3/2} q^2 \overline{\rho}^2/2\tau$ as reported in Figure 4.

For the third case study we have repeated the collisionality scan for a tokamak with large inverse aspect ratio, $a = 0.65\ m$, $R_0 = 0.85\ m$, B_0 =0.5 T and small ion Larmor radius ($\rho = 1.4\times10^{-3}$ m the thermal velocity being 3.4×10^4 ms^{-1}). The calculated diffusivities have been compared with the large aspect ratio limit neoclassical diffusion coefficients. Specifically, the neoclassical diffusion coefficients are those of particles having the same Larmor radius and collision time but placed in the field of a conventional tokamak on a surface having the same value of the cylindrical q as that calculated at the low field side of the tight aspect ratio plasma ($q_{out} = rB_t(R_{out})/B_pR_{out}$) under study, as illustrated in figure 5.

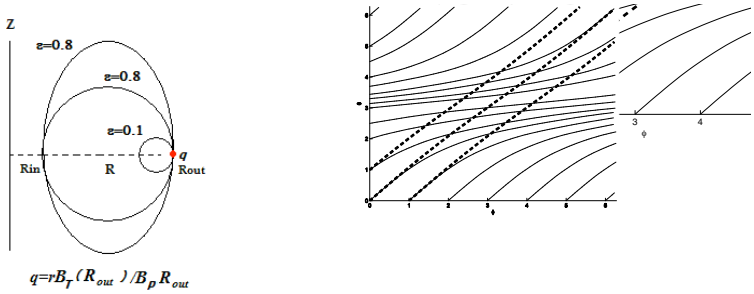

Figure 5. Magnetic field lines on a magnetic surface for ε=0.1 (dotted line) and ε=0.8 plotted in geometric angles. The field structure is chosen to coincide around $\theta = 0$ and $\theta = 2\pi$.

In Figure 6 the mean square displacement and the evolution of the radial distribution of the test particles initially located at mid radius (r_0 = 0.325 m), is shown for three high collisionality cases.

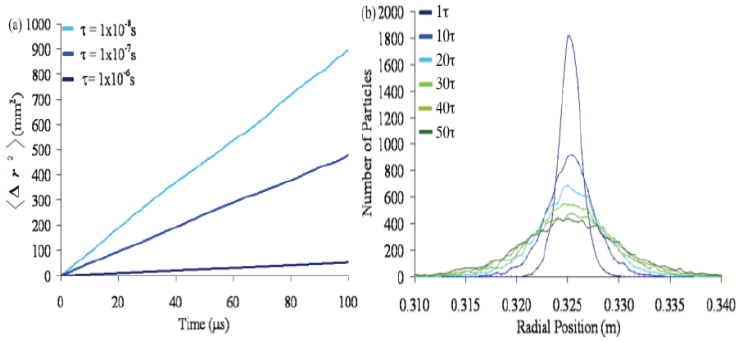

Figure 6. Mean square displacement of 10^4 particles (V_{th} = 3.4×10^4 ms^{-1}) for three high collision frequencies (left plot) and evolution of the radial particle distribution *with* $\tau = 8\times10^{-6}$ s (right).

kmcc 13/8/10 15:22

Comment: I'm puzzled by the numbers in Figs 6 and 7. For the longest collision time in Fig 6 (10^{-6}s) the slope of the line implies a diffusivity of about 0.25m^{2}s^{-1} but for the shortest collision time in Fig 7, which is 4 times longer, the diffusivity is actually higher, 0.35m^{2}s^{-1}. How can these numbers be consistent?

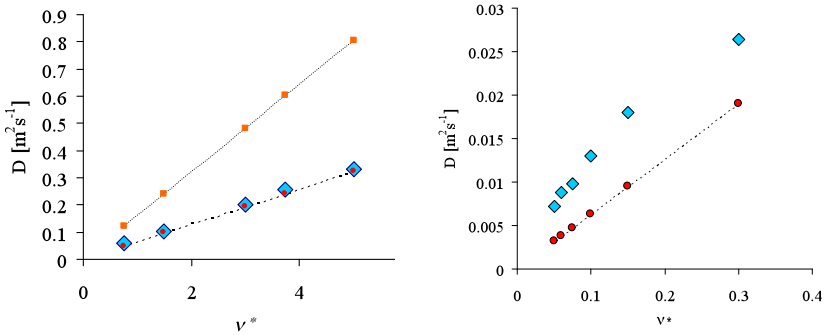

Figure 7. Scaling of the calculated diffusion coefficients (diamonds) with collisionality in the P-S (left plot) and Banana (right plot) regimes for small Larmor radius particles in a tight aspect ratio tokamak ($R_0/a=0.8$). Collision times range from 4×10^{-6} s to 2×10^{-3} s. The circles indicate the values of the analytical neoclassical P-S diffusion coefficient (left plot) and D_B (right plot) calculated with $q = q_{out}$ and ε=0.4. The square points in the left plot indicate the values of the P-S diffusion coefficient calculated taking $q=1.4$ (the flux surface average value).

The scaling of the diffusion coefficient with collisionality for this third case is shown in Figure 7. Increasing the collision time to approach the Pfirsch-Schlüter regime and plotting the mean radial displacement versus time, we find that two linear phases appear: initially the particles diffuse classically but later the diffusivity increases. The left plot of figure 7 shows the scaling with collisionality of the diffusion coefficient in the second diffusive region (diamonds) as compared with the P-S coefficient defined above (dots). The computed diffusivity found in the PS regime is lower than that calculated analytically taking the actual value of q at the initial magnetic surface (q = 1.4).
At the lowest collisionalities the effect of the finite orbits on the diffusive transport becomes apparent. Figure 8 shows the mean square radial displacement versus time for collision times 10^{-3} s, 2×10^{-3} s and 3×10^{-3} s. The mean square displacement does not increase linearly, hence the transport is non-diffusive; however we can define an effective diffusion coefficient as discussed above. Here, unlike in the high collisionality case, the diffusion coefficient can have a non monotonic dependence on collisionality and is not expected to agree with the analytical banana diffusion coefficient. Also shown in figure 8 is the evolution of the particle distribution for a simulation with $\tau = 10^{-3}$ s. A clear inward pinch was observed throughout the simulation; after 50 collision times the peak of the distribution had moved 55 mm inward from the initial position. It was observed that the Gaussian distribution became skewed towards the magnetic axis. The particles were spread radially over 0.25 m after a time of 50 ms, thus they travelled much further in 50 collision times than at higher collisionality.

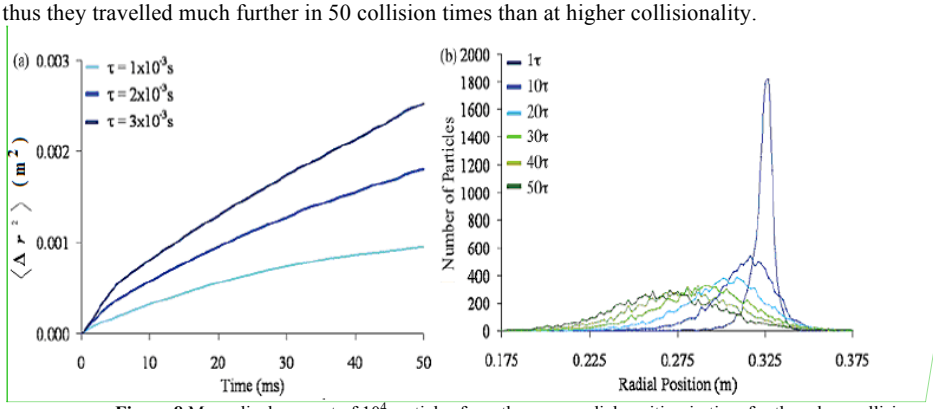

kmcc 13/8/10 14:59
Comment: The units in the left hand plot are clearly wrong since they would imply diffusivities of 10^{-7}m/s^2! Presumably the units should be m^2 not mm^2.

Figure 8 Mean displacement of 10^4 particles from the mean radial position in time for three low collision frequency cases and evolution of the radial particle distribution with collision time 10^{-3} s.

The estimated effective diffusion coefficient is shown in figure 9.

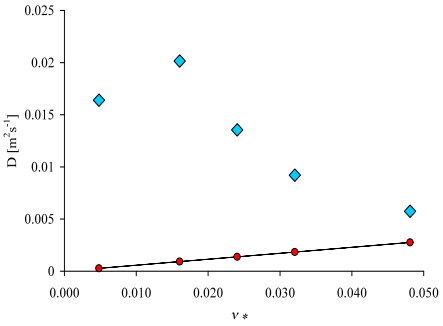

Figure 9. Scaling of the calculated diffusion coefficients (diamonds) vs collisionality in the banana regime for small Larmor radius ions in a tight aspect ratio tokamak ($R_0/a=0.8$). Collision times range from 1×10^{-3} s to 1×10^{-2} s. The circles indicate the values of D_B calculated with $q = q_{out}$ and ε=0.4.

In the fourth case study we calculated the transport of particles under the same conditions as case three, but with a thermal velocity of 4.8×10^5 ms^{-1} and initial positions r_0/a = 0.5 and r_0/a = 0.8. The results are similar to those illustrated in figure 8, namely non-diffusive transport at low collisionality dominated by a strong inward convection of particles. When initialized at r_0/a = 0.8 many particles are lost from the plasma within 50 collision times.

4. Effects of field fluctuations on ion transport

In the presence of field fluctuations (turbulence) it is no longer possible to define local transport coefficients, and particle transport becomes highly non-diffusive and non-local, subject as it is to particle advections in fields that are non uniform in both space and time [15-16]. Figure 10 shows the scattered trajectory of a test particle in MAST fields, simulated with CENTORI, followed until it is lost at r/a=0.95.

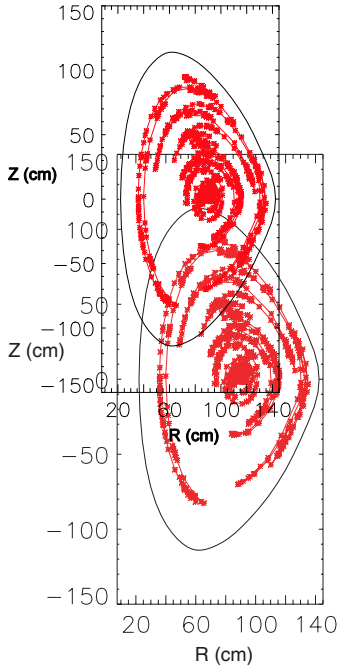

Figure 10. Particle orbit in MAST #18220, with fields calculated using CENTORI.

As a test case we have considered here the effect of fluctuations on the confinement of W^{20+} impurity ions in MAST conditions. The W ions were placed on the magnetic axis of an H-mode MAST-like rapidly rotating plasma with parameters close to those of shot number #18220 ($T_{e,i}$ = 0.6 keV, $n_e = 5\times10^{19}$m^{-3}, $\tau = 2.5\times10^{-5}$ s, ρ = 5.3 x10^{-3} m) and followed in the equilibrium and fluctuating fields. Particles which reached 95% of the minor radius were regarded as lost and removed from the simulation. If the transport were purely diffusive, the mean radial position of the set of particles would evolve on timescales much less than the confinement time according to the expression

$$\bar{r} = \frac{2\pi}{N_0}\int_0^\infty r^2 n(t,r)dr = \sqrt{\pi D t}\,.$$

As a first step we have analysed, in the above conditions, the collisional transport of W ions in the absence of fluctuations and radial electric fields. We followed the time evolution of the mean position

for approximately 25 ms. The W ions were transported on average a distance of 0.25 m from the magnetic axis (40% of the minor radius), and $\bar{r}$ exhibited a clear $t^{1/2}$ dependence, indicating a diffusivity of 1.1 m^2s^{-1} [15]. This is close to the expected P-S value in the plasma core, and implies a neoclassical confinement time of around 400 ms. No particles were lost in the 25 ms of this simulation.

Adding the equilibrium radial electric field and fluctuations as calculated by CUTIE for shot MAST #18220 and repeating the simulation we find that the W ions are transported much faster as a result of the combined effect of collisions, **E×B** drifts and fluctuating fields. As shown in figure 11 the W ions are on average transported across 95 % of the minor radius in 10 ms under the effect of the **E×B** drift only (figure 11, black curve) and in only 5 ms when fluctuations are included (blue curve). It is apparent from figure 11 that the transport process is non-diffusive.

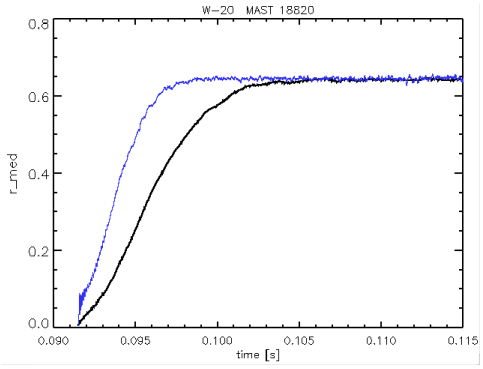

Figure 11. Mean position of 10^2 W particles in MAST plasma conditions after 25ms from injection and number of confined W ions versus time. Simulation of MAST #18220.Both radial electric field and fluctuations are included.

The confinement time of W^{20+} in MAST #18220 conditions is calculated by counting the lost particles and is found to be 16 ms. This is in agreement with the estimate of the energy confinement time in the CUTIE simulation (17 ms) and with experimental measurements.

5. Conclusions

The results of a numerical study on full orbit calculation of collisional and turbulent ion transport in MAST have been presented. The stochastic trajectories of a set of test particles have been determined in the equilibrium and simulated fluctuating electromagnetic fields of the MAST spherical tokamak using a full orbit code (CUEBIT). The fields have been computed with two independent two-fluid turbulence codes CUTIE and CENTORI. The test particles have been initialized on different magnetic surfaces and their local diffusion coefficient and convective velocity calculated from the time evolution of the radial distribution function. First CUEBIT was benchmarked for the case of collisional transport in the magnetic field of a large aspect ratio tokamak, with $\rho/a < 10^{-3}$. Numerical results for the scaling of diffusivity with collisionality have been shown to be generally in quantitative agreement with the predicted neoclassical scaling. Finite Larmor radius effects become important at low collisionalities for large ρ/a. It has been found that at the lowest collisionalities and for larger Larmor radii the advective velocity arising from the magnetic field non-uniformity coupled with collisions, moves the particles away from the initial magnetic surface before diffusion begins to dominate the process (non diffusive transport). In this context it is therefore in general not possible to define a strictly local diffusion coefficient for the more energetic ions even in a large aspect ratio tokamak. In the above case the fluxes have to be determined by a spatial average of the driving gradients in the neighbourhood of the initial magnetic surface. Finite orbit effects are found to be

important for thermal and energetic particles in the confining magnetic field of a tight aspect ratio tokamak at low collisionalities, where diffusion coefficients larger than neoclassical are found. At the lowest collisionalities advection dominates over diffusion and transport is non diffusive and non local. Strong advective velocities arise when the full fluctuating electromagnetic field of MAST is introduced in the problem. The effect of the electric field and fluctuations on the global confinement of impurities has been studied in the case of tungsten ions in a typical H-mode MAST discharge (shot #18820) where transport is found to be strongly enhanced by the presence of a strong radial electric field (consistent with the strong plasma rotation velocity), and the confinement time is reduced by a factor of about twenty by the combined effect of the equilibrium radial electric field and the fluctuating fields. In conclusion full orbit calculation of ion transport account for corrections over the neoclassical level of transport for thermal and energetic ions in a tight aspect ratio tokamak and energetic ions in a conventional tokamak. When the full equilibrium electric field, plasma velocity and electromagnetic fluctuations are taken into account the full orbit calculation produces particle confinement times in the range of those measured in the experiment.

This work was funded by the United Kingdom Engineering and Physical Sciences Research Council under grant EP/G003955 and the European Communities under the contract of Association between EURATOM and CCFE. The views and opinions expressed herein do not necessarily reflect those of the European Commission.

References

[1] Sykes A *et al* 2001 *Nucl. Fusion* **41** 1423
[2] Roach C M, Akers R J, Conway N J *et al* 2001 *Nucl. Fusion* **41** 11
[3] Synakowski E J *et al 2002 Plasma Phys. Control. Fusion* **44** A165
[4] Akers R J *et al 2003 Plasma Phys. Control. Fusion* **45** A175
[5] Helander P and Sigmar D J 2002 *Collisional Transport in Magnetized Plasma*, (Cambridge: Cambridge University Press)
[6] Wang W X, Rewoldt G, Tang W M *et al* 2006 *Phys. Plasmas* **13** 082501
[7] Gates, D A, Mynick H E and White R B 2004 *Phys. Plasmas* **11** L45
[8] McKay R J, McClements K G, Thyagaraja A and Fletcher L 2008 *Plasma Phys. Control. Fusion* **50** 065017
[9] Thyagaraja A *et al* 2005 *Phys. Plasmas* **12** 090907
[10] Thyagaraja A and Knight P J 2010 *Progress in Industrial Mathematics at ECMI 2008, Mathematics in Industry* **15** (Berlin: Springer-Verlag)
[11] Joiner N, Applegate D, Cowley S C *et al* 2006 *Plasma Phys. Control. Fusion* **48** 685
[12] Marmar E S, Cecchi J L, Cohen J A 1975 *Rev. Sci. Instrum.* **46** 1149
[13] Hamilton B, McClements K G, Fletcher L and Thyagaraja A 2003 *Solar. Phys.* ***214*** *339*
[14] McClements K G and McKay R J 2009 *Plasma Phys and Control. Fusion* **51** 115009
[15] Callaghan J, Romanelli M, Thyagaraja A and McClements K G 2009 *36th EPS Conf. on Plasma Physics (Sofia, Bulgaria)* vol 33E (ECA) P-4.109 (2009)
[16] Sánchez Burillo G, van Milligen B Ph and Thyagaraja A, 2009 *Phys. Plasmas* **16** 042319
[17] Cenacchi G and Taroni A 1998 *Rapporto* ENEA RT/TIB (88)5